



Metamaterials in multilayer graphene photonics: Control of negative refraction



Haixia Da ^{a, b, *}, Xiaohong Yan ^{a, b, c, **}

^a Nanjing University of Posts and Telecommunications, College of Electronic Science and Engineering, Nanjing, Jiangsu, 210046, China

^b Key Laboratory of Radio Frequency and Micro-Nano Electronics of Jiangsu Province, Nanjing, 210023, China

^c College of Science, Nanjing University of Aeronautics and Astronautics, Nanjing, Jiangsu, 210016, China

ARTICLE INFO

Article history:

Received 10 May 2015

Received in revised form

28 December 2015

Accepted 30 December 2015

Available online 4 January 2016

ABSTRACT

Negative refraction medium can in principle be realized using artificial composites composed of semiconductor/metallic inclusions, which experience negative refraction over certain frequency region due to structural resonant. It would be desirable if we could extend negative refraction to alternative natural semimetal candidates. Here, we show that by employing multilayer-graphene and cubic boron nitride slab, the composite may support negative group refractive angle over certain frequencies due to its anisotropic characteristics. Poynting vector profile numerically demonstrates that transverse magnetic wave propagates with observable negative shift as if they had negative refractive index.

© 2016 Elsevier Ltd. All rights reserved.

1. Introduction

In contrast to the well-known conventional refraction theory, negative refraction (NR) is a new concept which refers to the fact that the refraction and incident rays stay at the same side when the beam encounters the interface [1]. The experimental realization of this kind of materials in artificial structures has sparked considerable interest owing their fundamental new physics and potential applications in optical devices, such as subwavelength images, superlens and cloaking [2–8]. Existing proposals for realizing NR materials mainly rely on the conventional resonant-mediated mechanism [9–13]. By well designing subwavelength metamaterials, it is possible to achieve negative permittivity and permeability simultaneously at a certain frequency region owing to the possible resonances involved. Such a mechanism gives rise to NR properties within relatively complex geometrical structures, resulting in some difficulties in experimental fabrications. Apart from the above resonant mechanism, another scenario is proposed to create NR effect. It has been experimentally demonstrated that both two-dimensional metal wire and one-dimensional semiconductor multilayer structure support NR effect due to their

intrinsic strong anisotropy [14,15]. Such a scheme is based on multilayer structure and thus this will be relatively easy in fabrication.

Producing a controlled NR effect is a topic of central importance. The availability of an adjustable NR effect opens up the possibility of a much wider range of applications. The altering optical properties of metamaterials can be achieved by adding other components or engineering the geometrical configuration. For example, both experimental and theoretical investigations have revealed that tunable NR effect can be induced by photodoping a piece of low-doped semi-conductor positioned within the gap of the resonator, applying drops of silicon nanospheres to the split ring array, or photoexcitation of free carriers in the substrate [16–21]. From experimental perspective, however, the above schemes impose certain difficulty in fabrication. Therefore, the materials, which have intrinsic tunable optical properties, may serve as a platform for controllable optical devices by external means other than modifying geometrical configurations. The tunable functionality of the composite essentially relies on the sensitivity of permittivity/permeability on the external stimulus, enabling the controlled NR effect. Superconductor or ferromagnetic materials have been put forward to be the candidates, realizing tunable NR effect with the advantages of easiness of controllability, such as temperature or magnetic field [22–24]. But these approaches suffer from the transition from the superconductor/ferromagnetic state to normal conductor/paramagnetic state.

Graphene, a two-dimensional monolayer of carbon atoms

* Corresponding author. Nanjing University of Posts and Telecommunications, College of Electronic Science and Engineering, Nanjing, Jiangsu, 210046, China.

** Corresponding author. Nanjing University of Posts and Telecommunications, College of Electronic Science and Engineering, Nanjing, Jiangsu, 210046, China.

E-mail addresses: eledah@njupt.edu.cn (H. Da), yanxh@njupt.edu.cn (X. Yan).

arranged in a hexagonal lattice, has attracted great interest owing to its unusual electronic band structure [25]. The carriers of graphene are characterized by massless Dirac fermions, whose behaviors are governed by Dirac equation. The linear dispersion leads to its unique relativistic physical properties, such as integer and fractional quantum Hall effect, absence of backscattering and Klein tunneling [26–28]. Besides, graphene also exhibits fantastic optical properties owing to its unique optical conductivity. In this regard, graphene could be used to manipulate optical information because it is found to be extremely sensitive to external stimulus due to its ultrathin thickness. The AC conductivity of graphene has a strong dependence on chemical potential as well as magnetic field. Such a unique property of graphene makes it a promising candidate for tunable optical devices, including tunable plasmonics, gate-controlled active graphene metamaterials, transformation optics, cloaking, broadband polarizer, lens, giant Faraday rotation and optically transparent conductor [25–37].

It has been proposed that graphene with a well-designed optical conductivity distribution supports control of beam propagation, collimation, and focusing [38]. Therefore, one can imagine the possibility of tunable NR effect using carbon-based derivatives. In fact, the NR effect in thin graphite films has been advanced based on degenerate four-wave mixing [39]. In this approach, nonlinearity is the basic requirement to realize negative refractive angle. Graphite flakes with few graphene layers are used to lower the challenge in setting up the phase conjugation. This phenomenon reveals another unique optical property of graphite. However, the counter-propagating beams with strong electric fields are necessary due to the required nonlinearity, imposing the difficulty in experiment.

We know that the thickness is an important issue in designing the optical devices. However, the fixed thickness of graphene limits the direct applicability of the conventional optical effects to some extents. Increasing the layer number of graphene provides a possibility for overcoming this. In contrast to monolayer graphene, multilayer graphene has a more complex geometrical configuration because of different stacking sequences, which gets more rich physics and has its own contributions to optical fields due to the interlayer couplings. For example, gate tunable infrared phonon anomalies and an unusual giant Kerr effect have been reported in bilayer graphene due to the extra interlayer couplings between two layers [40,41]. The exploration of optical properties in few-layer graphene is still in early stage, which deserves more attention. It has been experimentally reported the lifetime of hot carriers in few-layer graphene appears to be longer than those in epitaxial graphene and graphite, indicating it is an important optoelectric material in high speed optoelectronics such as absorbers and modulators [42]. Besides, the optical transmittance of multilayer graphene can be modulated by means of an electrical signal in the simple configuration of coplanar electrodes [43]. Therefore, it offers new opportunities to explore an electrically controlled optical effect in terahertz metamaterials infiltrated with multilayer graphene. However, few reports concerning the tunable optical effects based on multilayer graphene have been presented in the literature.

Here we theoretically demonstrate a new mechanism for the chemical-potential manipulated NR effect. It can be realized by stacking multilayer graphene with Bernal sequence together where the spaces between the neighbor multilayer graphene are filled with dielectric materials, i.e., cubic boron nitride (BN). Owing to the Drude-like dynamics of multilayer graphene at low frequency regime, it provides the negative permittivity over a certain frequency. The existence of the multilayer graphene and BN slab lead to an effective anisotropic characteristic of the composite, whose anisotropic properties enable the observation of NR phenomenon.

The spatial-distributed field intensity and power distribution figures are a manifestation of anisotropic feature, where the NR happens at transverse magnetic polarization (TM) but not for transverse electric polarization (TE). In addition, similar to the single layer graphene, multilayer graphene is also sensitive to the gate voltage [44], thus the gate bias-sensitive NR is also investigated. Our results suggest that tunable NR effects are observed in multilayer graphene instead of single layer graphene. Importantly, this function can be extended to multilayer graphene with more layers and random orientation, making it more feasible for optical measurement in experiment. Thus, tunable NR effect can be realized by designing multilayer graphene with different layer numbers and stacking sequence other than nonlinearity, avoiding the need of strong incident pumps.

2. Methodology

A periodic structure is proposed which consists of alternating multilayer Bernal stacking graphene and dielectric materials as schematic figure shown in Fig. 1. The multilayer graphene lies in the x - y plane, which is separated by a normal dielectric BN slab. Multilayer Bernal stacking graphene is used as a candidate due to the fact that the same configuration with single layer graphene doesn't support NR properties (See Supplement file for details). BN is chosen as the spacer material due to the experimentally demonstrated good sample quality when graphene sits on it. z is propagating direction and a THz plane wave impinges upon the structure with an angle θ_i . A TM polarized light is a wave with the magnetic field perpendicular to the plane of incidence (xz), while TE polarized light is the wave with the electric field perpendicular to the plane of incidence. The thicknesses of multilayer graphene and BN slab are d_1 and d_2 , respectively. m is the repetition number of the structure.

The phase (θ_p) and group (θ_s) refractive angles are given by Ref. [45].

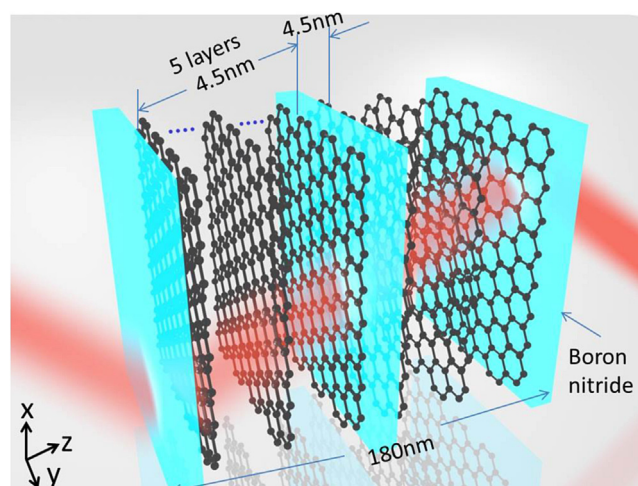


Fig. 1. Schematic of the negative refraction effect in multilayer graphene/cubic BN metamaterials. The sheets with black balls and lines show the schematic structure of multilayer graphene. The large space scale is taken for better visualization of multilayer graphene's geometry. Cubic BN is the spacer, which stacks with multilayer graphene alternatively. The thicknesses of multilayer graphene, cubic BN and total thickness of the stack are indicated in figures. An external gate voltage can be used to control the chemical potential of multilayer graphene. (A color version of this figure can be viewed online.)

$$\theta_p = \tan^{-1} \left(\frac{1}{d_t} \sum_{i=1}^m \int_0^{d_i} \frac{k_{xz}}{k_{zz}} dz \right) \quad (1)$$

$$\theta_s = \tan^{-1} \left(\frac{1}{d_t} \sum_{i=1}^m \int_0^{d_i} \frac{S_{xz}}{S_{zz}} dz \right)$$

where $d_t = m(d_1 + d_2)$ is the total thickness of the composite. k_{xz} is the tangential wave vector. k_{zz} is the wave vector along z direction,

which equals to $k_{zz} = \sqrt{\frac{\omega^2}{c^2} \epsilon_i - k_{xz}^2}$ ($k_{zz} = \sqrt{\frac{\omega^2}{c^2} \mu_i - k_{xz}^2}$) for TM (TE)

polarization, respectively. $S_{xz} = \frac{k_x H_y^2}{\omega \epsilon_i} \left(\frac{k_x E_y^2}{\omega \mu_i} \right)$ and $S_{zz} = \frac{k_z H_y^2}{\omega \epsilon_i} \frac{k_z E_y^2}{\omega \mu_i}$ are x

and z components of Poynting vector for TM (TE) mode, respectively, where E_y (H_y) are the electric (magnetic) field at the arbitrary position of z . They can be obtained from 2×2 transfer matrix method, which can be found elsewhere [46]. For comparison, we also calculate the phase and group refractive angle in the frame of effective medium theory (EMT) [14]. We know that PC structure can be treated as an effective anisotropic material with parallel and perpendicular permittivities in the long wave approximation, whose values are determined by $\epsilon_{\parallel} = \frac{\epsilon_1 d_1 + \epsilon_2 d_2}{d_1 + d_2}$ and $\frac{d_1 + d_2}{\epsilon_{\perp}} = \frac{d_1}{\epsilon_1} + \frac{d_2}{\epsilon_2}$, respectively. With these effective parameters, the wave vector and Poynting vector are easily obtained.

Regarding of multilayer graphene, five-layer graphene is chosen as an example and its AC-conductivity can be obtained by Kubo formula [47],

$$\sigma_{\alpha\beta}(\Omega) = \frac{e^2}{2\omega} \int_{-\infty}^{+\infty} \frac{d\omega}{2\pi} [f(\omega - \mu) - f(\omega + \Omega - \mu)] \int \frac{dk^2}{(2\pi)^2} \text{Tr} \left[v_{\alpha} A(\omega + \Omega, \vec{k}) v_{\beta} A(\omega, \vec{k}) \right], \quad (2)$$

($\alpha, \beta = x, y$), where $f(x) = \frac{1}{\exp(x/T) + 1}$ is the Fermi-Dirac function and T/μ is the temperature/chemical potential. Tr is the trace and $A(\omega)$ is the spectral function, connected to electronic Green's function $G_{ij}(z)$ by $G_{ij}(z) = \int_{-\infty}^{+\infty} \frac{d\omega}{2\pi} \frac{A_{ij}(\omega)}{z - \omega}$. $v_{\alpha\beta}$ is the velocity matrix which can be obtained by the derivatives of the Hamiltonian via Peierls substitution. The broadening parameter is assumed to be 1.3 meV and the temperature is chosen to be 10 K. Chemical potential (μ) is used to control the carrier density of the multilayer graphene. Here, the rigid band assumption is taken upon the application of different chemical potential [48]. For the spacer, the BN is just being used as a substrate which is made of cubic BN. The real and imaginary parts of the refractive index of cubic BN were obtained from the published data [49].

3. Results and discussions

In Fig. 2 we illustrate the dependence of θ_p and θ_g on frequency for TE (s) and TM (p) modes at $\theta_i = 60^\circ$, respectively. Here μ is taken to be 0.1 eV. For comparison, the results obtained from EMT are also shown in Fig. 2. The black (solid) and red (dash) lines represent θ_p and θ_g , respectively, while the blue (dotted) and green (dash dotted) are the results from EMT. It can be clearly observed that $\theta_{s,p}$ and $\theta_{s,g}$ increases first and remains almost the flat due to low phase and group refractive index at low frequency

region. They then drop sharply to 16.5° at a frequency of 48.8 THz. Beyond this point, θ_p and θ_g increase in the range of 48.8–70.9 THz and then decrease again. The variation of θ_p and θ_g are indicated by the change of phase and group refractive index. Obviously, $\theta_{s,p}$ and $\theta_{s,g}$ are positive and equal as shown in Fig. 2(a).

On the contrary, $\theta_{p,p}$ shows the similar behavior as the case of $\theta_{s,p}$ and it is positive. $\theta_{p,g}$ decreases a lot and then becomes zero at 40 THz. Remarkably, $\theta_{p,g}$ exhibits negative value over 40–44.09 THz for TM mode, which is known as group negative refraction. The fundamental dip occurs at 40.4 THz and has a negative value of -15.3° as shown by the red dashed line in Fig. 2(b). This is the key feature existing in the designed structure, which makes multilayer graphene potential candidates for NR effect at near-IR frequency region. We can see that the curves of θ_p and θ_g obtained from Eq. (1) and EMT are in coincidence with each other over a large frequency region including the negative group refraction region, which proves that EMT is effective to clarify the physics of negative group refraction behind. This allows us to directly elucidate all of the relevant electromagnetic parameters of the composite by EMT. It considerably simplifies our understanding on negative group refraction because there is no need to take into account the detailed interfaces.

In Fig. 2(c), we show the real and imaginary part of the AC conductivity of five-layer graphene at $\mu = 0.1$ eV. At low frequency where the intraband transition dominates, the real part of AC conductivity $\text{Re}[\sigma]$ decays rapidly and the imaginary part of AC conductivity $\text{Im}[\sigma]$ is positive, which exhibits a typical Drude-like behavior. After a flat region in $\text{Re}[\sigma]$, the interband transition overwhelms, where a small jump in $\text{Re}[\sigma]$ occurs and the negative $\text{Im}[\sigma]$ can be seen. Besides, the magnitude of $\text{Re}[\sigma]$ is less than 1 over a large frequency region in five-layer graphene, indicating its small imaginary part of permittivity and low loss. Fig. 2(d) shows the calculated real parts of the effective parallel and perpendicular permittivities by EMT as a function of frequency, respectively. As observed, it first increases from negative value and then decreases with the frequency increasing in $\text{Re}[\epsilon_{\parallel}]$ and there is a hump corresponding to negative dip in $\text{Im}[\sigma]$. Especially, the transition point between negative and positive values happens at the frequency of 40 THz. Obviously, $\text{Re}[\epsilon_{\perp}]$ first increases to a large positive value, which decreases to negative value at the same frequency of 40 THz. With the further increase of frequency, $\text{Re}[\epsilon_{\perp}]$ becomes positive value again. There is a region with simultaneously positive $\text{Re}[\epsilon_{\parallel}]$ and negative $\text{Re}[\epsilon_{\perp}]$, which is in accord with the regime with negative $\theta_{p,g}$. It is useful to identify the NR regime. The large carrier mobility of multilayer graphene makes its intrinsic loss lower than that of the metals. Therefore, the capability of five-layer graphene equipped with the combination of its low loss and ultrathin thickness enables the electromagnetic wave propagation in an unusual way, i.e., NR effect.

It is well known that negative refraction effect can be understood in terms of Poynting vector, which does not always align with the direction of wave vector illustrated in reported anisotropic NRI materials [14]. Such a feature is used to judge whether materials exhibit NR properties. For the effective uniaxial anisotropic material, the Poynting vectors of TE and TM modes read [50].

$$\vec{S}_{TE} = \frac{|E_0|^2}{2\omega} \left[\frac{k_x}{\mu_1} \vec{e}_x + \frac{k_z}{\mu_1} \vec{e}_z \right], \quad (3)$$

$$\vec{S}_{TM} = \frac{|E_0|^2}{2\omega} \left[\frac{k_x}{\epsilon_{\perp}} \vec{e}_x + \frac{k_z}{\epsilon_{\parallel}} \vec{e}_z \right], \quad (4)$$

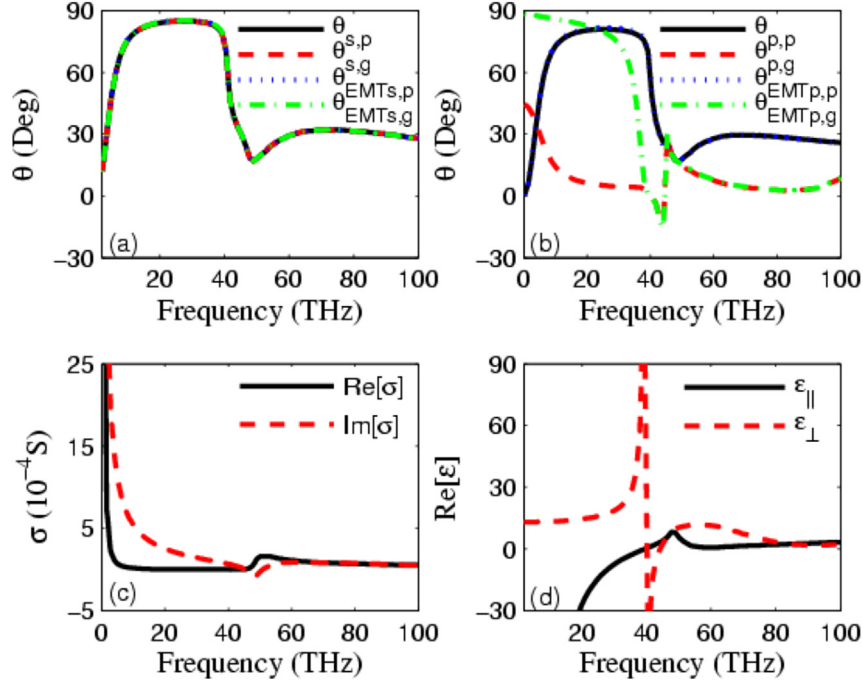


Fig. 2. Phase and group refractive angles in five-layer graphene/cubic BN metamaterial. (a) Phase ($\theta_{s,p}$) and group ($\theta_{s,g}$) refractive angles versus frequency for TE mode (b) Phase ($\theta_{p,p}$) and group ($\theta_{p,g}$) refractive angles versus frequency for TM mode. The black solid and red dot lines are the phase and group refractive angles, respectively. Blue dot and green dashed dot lines are the results from EMT. (c) Real (black solid line) and imaginary (red dot line) parts of AC conductivity versus frequency for five-layer graphene, which are obtained from Kubo formula. (d) The real parts of the effective parallel (black solid line) and perpendicular permittivities (red dash line) versus frequency obtained from EMT, respectively. In (a)–(d), thickness of cubic-BN is 4.5 nm and the chemical potential is set to be 0.1 eV. (A color version of this figure can be viewed online.)

Note that the energy flow should propagate forward and thus it requires the signs of the Poynting vector along the normal direction should be continuous. In our cases, that is to say $\vec{e}_z \cdot \vec{S} > 0$. Therefore, the tangential direction of the Poynting vector dominates that the refraction is positive or negative. Based on this argument, obviously, TE mode only involves in permeability and thus it is isotropic, implying we have equal and positive θ_k and θ_s for TE mode. The case is totally different for TM mode. The coexistence of ϵ_{\parallel} and ϵ_{\perp} determines its anisotropic properties. It is clear that the sign of z component of Poynting vector depends only on the term k_z/ϵ_{\parallel} , illustrating that the sign of k_z and ϵ_{\parallel} should be the same to satisfy the above requirement. Then ϵ_{\parallel} is positive/negative and k_z must be positive/negative, indicating its positive/negative phase refraction. On the contrary, the sign of k_x/ϵ_{\perp} , i.e., ϵ_{\perp} is thus vital to determine the sign of group refraction. As illustrated in Fig. 2 (d), the region of negative ϵ_{\perp} is exactly coincidence with that of negative group refraction for TM mode and positive ϵ_{\parallel} results in positive phase refraction.

To further validate our claim that the NR here originates from the sign of effective ϵ_{\perp} , the electric field distribution and time-averaged power density are instructive to identify the possible NR effect upon the Gauss-shaped illumination. It can be calculated based on the electric (or magnetic) field profile at the incident medium for TM (TE) mode, which is written by $H_{0y} = \int_{-\infty}^{+\infty} d_{k_x} \phi(k_x) e^{ik_x x + ik_{0z} z}$ ($E_{0y} = \int_{-\infty}^{+\infty} d_{k_x} \phi(k_x) e^{ik_x x + ik_{0z} z}$), where $\phi = \frac{g}{2\sqrt{\pi}} e^{-\frac{g^2(k_x - k_{ix})^2}{4}}$ is the Gaussian spectrum and it carries the information of the shape of the footprint at $x = z = 0$. $k_{ix} = \frac{\omega}{c} \sqrt{\epsilon_0 \mu_0} \sin \theta_i$ is the angle of the center of the incident wave, ω is the angular frequency of incident wave and c stands for the velocity of the light

in the vacuum. The magnetic and electric fields in the incident medium for TM mode are given by Ref. [50].

$$\begin{aligned}
 H_{iy} &= \int_{-\infty}^{+\infty} d_{k_x} \phi(k_x) \left[e^{ik_{iz}z} + Re^{-ik_{iz}z} \right] e^{ik_x x} \\
 E_{ix} &= \int_{-\infty}^{+\infty} d_{k_x} \phi(k_x) \frac{k_{iz}}{\omega \epsilon_1} \left[e^{ik_{iz}z} - Re^{-ik_{iz}z} \right] e^{ik_x x} \\
 E_{iz} &= \int_{-\infty}^{+\infty} d_{k_x} \phi(k_x) \frac{-k_x}{\omega \epsilon_1} \left[e^{ik_{iz}z} + Re^{-ik_{iz}z} \right] e^{ik_x x}
 \end{aligned} \quad (5)$$

In the region where the five-layer graphene or cubic BN occupies, the electric and magnetic fields can be written as

$$\begin{aligned}
 H_{jy} &= \int_{-\infty}^{+\infty} d_{k_x} \phi(k_x) \left[A_j e^{ik_{jz}z} + B_j e^{-ik_{jz}z} \right] e^{ik_x x} \\
 E_{jx} &= \int_{-\infty}^{+\infty} d_{k_x} \phi(k_x) \frac{k_z}{\omega \epsilon_j} \left[A_j e^{ik_{jz}z} - B_j e^{-ik_{jz}z} \right] e^{ik_x x} \\
 E_{jz} &= \int_{-\infty}^{+\infty} d_{k_x} \phi(k_x) \frac{-k_x}{\omega \epsilon_j} \left[A_j e^{ik_{jz}z} + B_j e^{-ik_{jz}z} \right] e^{ik_x x}
 \end{aligned} \quad (6)$$

In the outgoing medium, the electric and magnetic fields take the form,

$$\begin{aligned}
 H_{ty} &= \int_{-\infty}^{+\infty} d_{k_x} \phi(k_x) [T e^{ik_{iz}z}] e^{ik_x x} \\
 E_{tx} &= \int_{-\infty}^{+\infty} d_{k_x} \phi(k_x) \frac{k_{tz}}{\omega \epsilon_t} [T e^{ik_{iz}z}] e^{ik_x x} \\
 E_{tz} &= \int_{-\infty}^{+\infty} d_{k_x} \phi(k_x) \frac{-k_x}{\omega \epsilon_t} [T e^{ik_{iz}z}] e^{ik_x x}
 \end{aligned} \quad (7)$$

where $k_{iz}(\epsilon_i)$, $k_{jz}(\epsilon_j)$, $k_{tz}(\epsilon_t)$ are z-component of the wave vectors (permittivities) in the incident, j-component, outgoing media, respectively. The coefficients of R, T, A_j, B_j are the reflection, transmission coefficients, the amplitudes of magnetic field for forward and backward waves in j-component, respectively. These can be determined by the transfer matrix method [46]. Along with the electric and magnetic fields distribution in all regions, the time-average Poynting vector can be calculated via $|\langle \vec{S}_n \rangle| = \frac{1}{2} \sqrt{[\text{Re}(E_{nx} H_{ny}^*)]^2 + [\text{Re}(E_{nz} H_{ny}^*)]^2}$, where $n = i, j, t$ stands for the incident, j-component and outgoing regions, respectively. The case for TE mode can be treated similarly by replacing the permittivity with the corresponding permeability.

Fig. 3(a)–(d) show the calculated electric-field profile obtained from Eqs. (5)–(7) and time-averaged power density of the incident wave transmitted by the composite with the map of the electric-field distribution in x-z plane at $\theta_i = 30^\circ$. From the electric field distribution and power density, it can be found that the center of output TM wave exhibits negative lateral shift compared with that of incident wave when propagating through the composite,

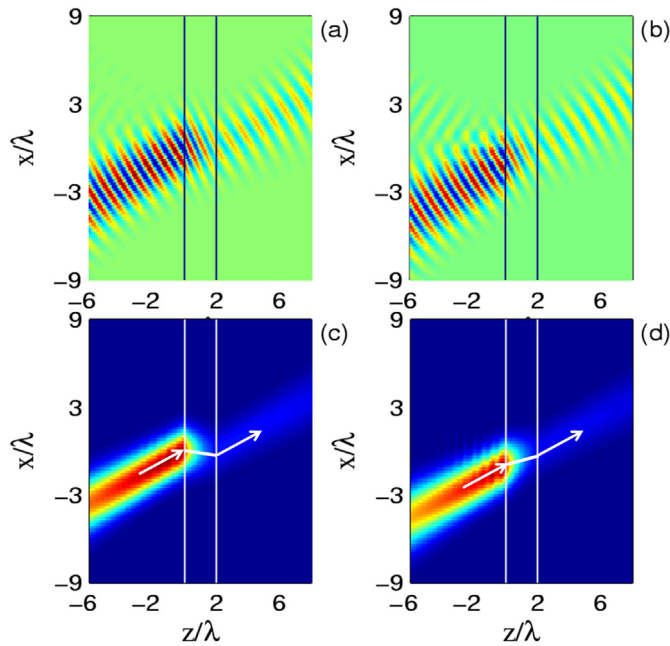


Fig. 3. Illustration of negative refraction by electric field intensity and power density distribution. Calculated electric field distribution (a) for TM mode (b) for TE mode in five-layer graphene/cubic BN stacks; The power density distribution (c) for TM mode (d) for TE mode. The arrows indicate the shift of the outgoing Gaussian beam and vertical solid line represents the edges where the composite covers. In (a)–(d), the chemical potential is $\mu = 0.1$ eV. The specified frequency is $f = 41.68$ THz, which is randomly chosen from the region where NR happens. The similar profile is observed at other frequencies with negative $\theta_{p,g}$. The mesh resolution was 0.09 nm along the propagation direction. (A color version of this figure can be viewed online.)

indicating its negative group refraction, while the TE wave experiences positive lateral shift and thus positive group refraction when it transmits through the composite. Thus, the interaction between the TE mode and the composite eludes the possibility of NR effect. This is in good agreement with the previously theoretical description due to the anisotropic spatial dispersion of the effective composite. Thus it proves that an interface between air and the effective uniaxial composite supports negative group refraction for TM mode when $\epsilon_{\perp} < 0$ condition is satisfied. This is an important confirmation of the theoretical predictions of negative group refraction, demonstrating that the NR can be achieved in multilayer graphene-based composite apart from semiconductor/metal components. With increasing total thickness of the composite, the negative lateral shift will be more significant. It can be ascribed to the fact that the lateral shift is strongly dependent on the distance light travels, which would be helpful for experimental observations.

Moving further, we study the interaction between light and the effective composite under different chemical potential μ . The combination of unique dispersion relationship and few atomic layer thickness of multilayer graphene determines that the chemical potential can be fine controlled by electrostatic gating or chemical doping. Fig. 4(a) displays the group refractive angle of the TM mode as a function of frequency and incident angle at various $\mu = 0.1, 0.2$ and 0.3 eV, respectively. We can see that there is no NR region at $\theta_i = 0^\circ$ and NR region is almost invisible at low incident angle. With incident angle increasing, a region of negative group refractive angle for TM mode appears. The frequency range of NR keeps unchanged but the amplitude of the maximum NR angle gets larger with an increased incident angle. Fig. 4 (b) and (c) shows the chemical-potential modulation on $\theta_{p,g}$ for TM mode at $\mu = 0.2$ and 0.3 eV, respectively. It can be observed that the curves show similar behaviors but with modulated peak values and shifted peak positions in $\theta_{p,g}$ under different μ . At an increased chemical potential $\mu = 0.2$ eV, the region with negative $\theta_{p,g}$ gets larger from 40 to 59.9 THz and the magnitude of the maximum NR angle approaches -73.1° . In addition, the position of the maximum negative refractive angle is shifted to higher frequencies. With the further increase of μ , the region of negative $\theta_{p,g}$ shifts towards low frequency which occurs at the frequency of 36–57.5 THz and the maximum negative refractive angle slightly gets smaller. This dependence of $\theta_{p,g}$ on the chemical potential can be ascribed to the unique properties multilayer graphene has. The variation of $\theta_{p,g}$ originates from the change in AC conductivity of multilayer graphene and thus the effective permittivity parameter, which leads to the variation in the magnitude and the shift in the position of the maximum $\theta_{p,g}$. This chemical potential-controlled NR effect enables wide applications in multilayer graphene-based structures, distinguishing this PC composed of multilayer graphene from that composed of conventional metal.

The currently existing NR devices mainly rely on the components of metal or semiconductor. We know that the optical properties of most metals are hard to control if the composition or geometry of the nanostructures stays the same. In contrast to conventional NR produced by metal bulky materials or nanowires, the NR effect introduced by multilayer graphene in our devised structure is strongly sensitive to external stimulus, such as chemical potential or strain, exhibiting a controllable NR response. In addition, semiconductors support temperature-controlled optical properties, but the carrier mobility in conventional semiconductors is low at room temperature and high carrier density. These inherent drawbacks of metal and semiconductors impose serious restrictions to the applications in tunable optoelectronics. Unlike the NR devices made of metal/semiconductor materials, our configuration is capable of generating tunable NR effect even at room

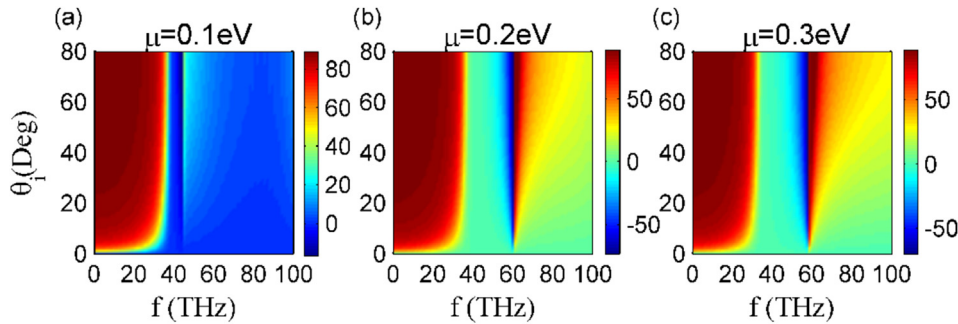


Fig. 4. Group refractive angle θ_{pg} for TM mode as functions of frequency and incident angle at different chemical potential (a) $\mu = 0.1$ eV, (b) $\mu = 0.2$ eV and (c) $\mu = 0.3$ eV, respectively. The color bar indicates the value of θ_{pg} with a unit of degree and is applied to all plots. (A color version of this figure can be viewed online.)

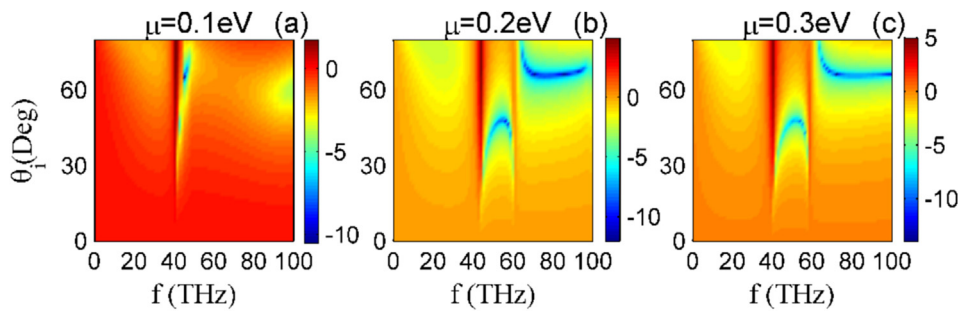


Fig. 5. The ratio of reflectance between TM and TE modes, $\log(R_{TM}/R_{TE})$, as functions of frequency and incident angle at different chemical potential (a) $\mu = 0.1$, (b) 0.2 and (c) 0.3 eV, respectively. The color bar indicates the value of $\log(R_{TM}/R_{TE})$ and is applied to all plots. The discontinuous region indicates its NR regime. (A color version of this figure can be viewed online.)

temperature in which those established methods are not able to function competitively. It can be ascribed to the fact that the carbon-based family, such as graphene and multilayer graphene, provide large tunability and outstanding carrier mobility. Therefore, our proposed scheme offers a promising avenue to realize NR effects using multilayer graphene.

Power density distribution is vital to demonstrate the existence of NR effect. From experimental point of view, the transmission and/or reflectance spectrum is also instructive to identify when negative group refraction happens. In our cases, the ratio of TM/TE reflectance spectrum has a more clear indication of NR effect compared with the case of transmission. We thus plot the ratios of TM/TE reflectance spectrum of the stacking configuration as a function of frequency under different incident angle and chemical potential in a logarithmic scale in Fig. 5. It can be observed that an obvious narrow region appears around 40 THz in the $\log(R_{TM}/R_{TE})$ at $\mu = 0.1$ eV and $\log(R_{TM}/R_{TE})$ exhibits a clear and wider range with an increased μ , which corresponds to the region with NR effect in TM mode described above. This can be explained as: when the working frequency approaches the frequency with $\varepsilon_{\perp} = 0$, the TM mode experiences a high reflection peak at this position and the associated frequency dependence of the TE mode has no observable feature, thus determining the right edge of NR effect [14]. The left edge is revealed by the transition point between positive and negative value in ε_{\perp} . The characteristics of reflectance spectrum allow to directly assessing the region with negative group refractive angle. We like to emphasize that our conclusion does not necessarily limited by multilayer graphene with Bernal stacking, which can be extended to other stacking orders with semimetal properties. Experiments have shown that the misaligned multilayer graphene exhibits such features single layer graphene has [51]. Therefore, NR is also expected in misaligned multilayer graphene, lowering the fabrication difficulty

and making NR effect more available in experiments.

4. Conclusion

In this work, we introduced an adjustable NR effect operating at terahertz frequencies in multilayer graphene-based configuration. The previously proposed models composed of conventional semiconductor/metal slab favoring NR effect cannot be applied to single-layer graphene, but holds true for multilayer graphene models. The phase and group refraction are the same under excited TE polarized light due to the isotropic characteristics. The negative group refraction for TM mode has clearly been identified theoretically due to the anisotropic features in the composite with a demonstration by the results of the distribution of electric field profile and Poynting vector. In addition, we observe a sensitive dependence on the gate voltage and a shift of the negative group refraction, enabling tunable optical devices with multilayer graphene.

Acknowledgment

This project was sponsored by NUPTSF (Grant No. NY215027), the National Natural Science Foundation of China (NSFC11374162) and Major Program of Natural Science Foundation by the Ministry of Education of China (TJ215009).

Appendix A. Supplementary data

Supplementary data related to this article can be found at <http://dx.doi.org/10.1016/j.carbon.2015.12.097>.

References

- [1] V.G. Veselago, *Soviet Phys. Uspekhi* 10 (1968) 509.
- [2] Zhaolin Lu, Janusz A. Murakowski, Christopher A. Schuetz, Shouyuan Shi, Garrett J. Schneider, Dennis W. Prather, *Phys. Rev. Lett.* 95 (2005) 153901.
- [3] N. Fang, H. Lee, C. Sun, X. Zhang, *Science* 308 (2005) 534.
- [4] Z. Liu, H. Lee, Y. Xiong, C. Sun, X. Zhang, *Science* 315 (2007) 1686.
- [5] J.B. Pendry, *Phys. Rev. Lett.* 85 (2000) 3966.
- [6] Baile Zhang, Bae-Ian Wu, *Phys. Rev. Lett.* 103 (2009) 243901.
- [7] D. Schurig, J.J. Mock, B.J. Justice, S.A. Cummer, J.B. Pendry, A.F. Starr, D.R. Smith, *Science* 314 (2006) 977.
- [8] Stanley P. Burgos, Rene deWaele, Albert Polman, Harry A. Atwater, *Nat. Mater.* 9 (2010) 407.
- [9] R.A. Shelby, D.R. Smith, S. Schultz, *Science* 292 (2001) 77.
- [10] D.R. Smith, W.J. Padilla, D.C. Vier, S.C. Nemat-Nasser, S. Schultz, *Phys. Rev. Lett.* 84 (2000) 4184.
- [11] J.B. Pendry, D.R. Smith, *Phys. Today* 57 (2004) 37.
- [12] J. Valentine, S. Zhang, T. Zentgraf, E. Ulin-Avila, D.A. Genov, G. Bartal, X. Zhang, *Nature* 455 (2008) 376.
- [13] S. Zhang, W. Fan, B.K. Minhas, A. Frauenglass, K.J. Malloy, S.R.J. Brueck, *Phys. Rev. Lett.* 94 (2005) 037402.
- [14] Jie Yao, Zhaowei Liu, Yongmin Liu, Yuan Wang, Cheng Sun, Guy Bartal, Angelica M. Stacy, Xiang Zhang, *Science* 321 (2008) 920.
- [15] Anthony J. Hoffman, Leonid Alekseyev, Scott S. Howard, Kale J. Franz, Dan Wasserman, Viktor A. Podolskiy, Evgenii E. Narimanov, Deborah L. Sivco, Claire Gmachl, *Nat. Mater.* 6 (2007) 946.
- [16] T. Driscoll, G.O. Andreev, D.N. Basov, S. Palit, S.Y. Cho, N.M. Jokerst, D.R. Smith, *Appl. Phys. Lett.* 91 (2007) 062511.
- [17] W.J. Padilla, A.J. Taylor, C. Highstrete, M. Lee, R.D. Averitt, *Phys. Rev. Lett.* 96 (2007) 107401.
- [18] A. Degiron, J.J. Mock, D.R. Smith, *Opt. Express* 15 (2007) 1115.
- [19] D.X. Wang, L.X. Ran, H.S. Chen, M.K. Mu, J.A. Kong, B.I. Wu, *Appl. Phys. Lett.* 91 (2007) 164101.
- [20] H.S. Chen, B.I. Wu, L.X. Ran, T.M. Grzegorzczak, J.A. Kong, *Appl. Phys. Lett.* 89 (2006) 053509.
- [21] A.W. Clark, A.K. Sheridan, A. Gildle, D.R.S. Cumming, J.M. Cooper, *Appl. Phys. Lett.* 91 (2007) 093109.
- [22] Shiyang Liu, Weikang Chen, Junjie Du, Zhifang Lin, S.T. Chui, C.T. Chan, *Phys. Rev. Lett.* 101 (2008) 157407.
- [23] A. Pimenov, A. Loidl, P. Przyślupski, B. Dabrowski, *Phys. Rev. Lett.* 95 (2005) 247009.
- [24] A. Pimenov, A. Loidl, K. Gehrke, V. Moshnyaga, K. Samwer, *Phys. Rev. Lett.* 98 (2007) 197401.
- [25] A. Bostwick, T. Ohta, T. Seyller, K. Horn, E. Rotenberg, *Nat. Phys.* 3 (2007) 36.
- [26] C.R. Dean, A.F. Young, P. Cadden-Zimansky, L. Wang, H. Ren, K. Watanabe, T. Taniguchi, P. Kim, J. Hone, K.L. Shepard, *Nat. Phys.* 7 (2011) 693.
- [27] A. Cresti, M.M. Fogler, F. Guinea, A.H. Castro Neto, S. Roche, *Phys. Rev. Lett.* 108 (2012) 166602.
- [28] M.I. Katsnelson, K.S. Novoselov, A.K. Geim, *Nat. Phys.* 2 (2006) 620.
- [29] F. Bonaccorso, Z. Sun, T. Hasan, A.C. Ferrari, *Nat. Photonics* 4 (2010) 611.
- [30] Yuanbo Zhang, Yan-Wen Tan, Horst L. Stormer, Philip Kim, *Nature* 438 (2005) 201.
- [31] Qiaoliang Bao, Han Zhang, Bing Wang, Zhenhua Ni, Candy Haley Yi Xuan Lim, Yu Wang, Ding Yuan Tang, Kian Ping Loh, *Nat. Photonics* 5 (2011) 411.
- [32] Ashkan Vakil, Nader Engheta, *Science* 332 (2011) 1291.
- [33] Ming Liu, Xiaobo Yin, Erick Ulin-Avila, Baisong Geng, Thomas Zentgraf, Long Ju, Feng Wang, Xiang Zhang, *Nature* 474 (2011) 64.
- [34] Vadim V. Cheianov, Vladimir Falko, B.L. Altshuler, *Science* 315 (2007) 1252.
- [35] Pai-Yen Chen, Andrea Alu, *ACS Nano* 5 (2011) 5855.
- [36] I. Crassee, J. Levallois, A.L. Walter, M. Ostler, A. Bostwick, E. Rotenberg, T. Seyller, D. van derMarel, A.B. Kuzmenko, *Nat. Phys.* 7 (2010) 24748.
- [37] Kian Ping Loh, Qiaoliang Bao, Goki Eda, Manish Chhowalla, *Nat. Chem.* 2 (2010) 1015.
- [38] Zhengfei Wang, Feng Liu, *ACS Nano* 4 (2010) 2459.
- [39] Hayk Harutyunyan, Ryan Beams, Lukas Novotny, *Nat. Phys.* 9 (2013) 423.
- [40] H.G. Yan, T. Low, F. Guinea, F.N. Xia, P. Avouris, *Nano Lett.* 14 (2014) 4581.
- [41] R. Nandkishore, L. Levitov, *Phys. Rev. Lett.* 107 (2011) 097402.
- [42] Thomas Limmer, Jochen Feldmann, Enrico Da Como, *Phys. Rev. Lett.* 110 (2013) 217406.
- [43] J.L. Benitez, D. Mendozaa, *Appl. Phys. Lett.* 103 (2013) 083116.
- [44] Maxim Trushin, John Schliemann, *New J. Phys.* 14 (2012) 095005.
- [45] Ivan D. Rukhlenko, Malin Premaratne, Govind P. Agrawal, *Opt. Exp.* 18 (2010) 279.
- [46] K. Busch, C.T. Chan, C.M. Soukoulis, in: C.M. Soukoulis (Ed.), *Photonic Band Gap Materials*, Kluwer, Dordrecht, 1996.
- [47] V.P. Gusynin, S.G. Sharapov, *Phys. Rev. B* 73 (2006) 245411.
- [48] Chun Hung Lui, Emmanuele Cappelluti, Zhiqiang Li, Tony F. Heinz, *Phys. Rev. Lett.* 110 (2013) 185504.
- [49] Yong-Nian Xu, W.Y. Ching, *Phys. Rev. B* 44 (1991) 7787.
- [50] H.X. Da, C. Xu, Z.Y. Li, *Phys. Rev. E* 71 (2005) 066612.
- [51] Giuseppe Pirruccio, Luis Martín Moreno, Gabriel Lozano, Jaime Gomez Rivas, *ACS Nano* 7 (2013) 4810.